Multidecadal Indian Ocean Variability Linked to the Pacific and Implications for Preconditioning Indian Ocean Dipole Events

CAROLINE C. UMMENHOFER

Department of Physical Oceanography, Woods Hole Oceanographic Institution, Woods Hole, Massachusetts

ARNE BIASTOCH AND CLAUS W. BÖNING

GEOMAR Helmholtz Centre for Ocean Research Kiel, Kiel, Germany

ABSTRACT

The Indian Ocean has sustained robust surface warming in recent decades, but the role of multidecadal variability remains unclear. Using ocean model hindcasts, characteristics of low-frequency Indian Ocean temperature variations are explored. Simulated upper-ocean temperature changes across the Indian Ocean in the hindcast are consistent with those recorded in observational products and ocean reanalyses. Indian Ocean temperatures exhibit strong warming trends since the 1950s limited to the surface and south of 30°S, while extensive subsurface cooling occurs over much of the tropical Indian Ocean. Previous work focused on diagnosing causes of these long-term trends in the Indian Ocean over the second half of the twentieth century. Instead, the temporal evolution of Indian Ocean subsurface heat content is shown here to reveal distinct multidecadal variations associated with the Pacific decadal oscillation, and the long-term trends are thus interpreted to result from aliasing of the low-frequency variability. Transmission of the multidecadal signal occurs via an oceanic pathway through the Indonesian Throughflow and is manifest across the Indian Ocean centered along 12°S as westward-propagating Rossby waves modulating thermocline and subsurface heat content variations. Resulting low-frequency changes in the eastern Indian Ocean thermocline depth are associated with decadal variations in the frequency of Indian Ocean dipole (IOD) events, with positive IOD events unusually common in the 1960s and 1990s with a relatively shallow thermocline. In contrast, the deeper thermocline depth in the 1970s and 1980s is associated with frequent negative IOD and rare positive IOD events. Changes in Pacific wind forcing in recent decades and associated rapid increases in Indian Ocean subsurface heat content can thus affect the basin's leading mode of variability, with implications for regional climate and vulnerable societies in surrounding countries.

1. Introduction

Changes over the past two decades in upper-ocean temperatures in the Indian Ocean have recently received increasing attention (e.g., Vialard 2015). The Indian Ocean 100–300-m depth layer has warmed significantly since 2003 (Nieves et al. 2015). Rapid increases are also seen in the top 700-m Indian Ocean heat content since the early 2000s (Lee et al. 2015), concurrent with an increased heat transport from the Pacific to the Indian Ocean through the Indonesian Throughflow (ITF), following enhanced Pacific Ocean heat uptake. The latter had been implicated in recent slower global

surface temperature increases during a sustained cooling period in the equatorial Pacific associated with a negative phase of the interdecadal Pacific oscillation (IPO; e.g., Kosaka and Xie 2013; England et al. 2014). Lee et al. (2015) proposed that the rapid increase in Indian Ocean heat content accounted for more than 70% of the global upper 700-m heat content gain during the past decade. Given these rapid changes underway in the Indian Ocean and their implications for global climate, it is of interest to better understand low-frequency behavior in upper-ocean thermal properties in the Indian Ocean over past decades. Here, we assess multidecadal variations in the Indo-Pacific using high-resolution ocean general circulation model (OGCM) hindcasts to provide a longer context for the recent upper-ocean thermal changes in the Indian Ocean. This

Corresponding author e-mail: Caroline C. Ummenhofer, cummenhofer@whoi.edu

is important for understanding whether recent Indian Ocean temperature changes reflect long-term trends (e.g., Alory et al. 2007; Cai et al. 2008) or whether they are a manifestation of decadal and/or multidecadal variability. We also evaluate whether Indo-Pacific background changes on such time scales have implications for interannual Indian Ocean variability.

Tropical Indian Ocean sea surface temperature (SST) generally warmed faster during the period 1950–2010 than the tropical Atlantic or Pacific (Han et al. 2014a). In particular western Indian Ocean SST have warmed by 1.2°C over the period 1901–2012, making the western Indian Ocean the largest contributor to the overall global SST trend (Roxy et al. 2014). Schott et al. (2009) considered the Indian Ocean SST warming trend to exhibit "puzzling subbasin-scale features which are difficult to explain with surface heating alone." Considerable uncertainty exists about the sign of the net heat flux into or out of the Indian Ocean in some parts (Yu et al. 2007); best estimates do not indicate an increase in heat flux into the Indian Ocean but a likely negative heat flux trend unable to explain surface warming (Schott et al. 2009). In contrast, Alory and Meyers (2009) attributed the surface warming to a decrease in upwelling-related ocean cooling over the thermocline dome region, arising from reduced wind-driven Ekman pumping; a negative heat flux results, driven by a negative feedback through evaporation, compounded by strengthening trade winds resulting from equatorial warming. As summarized by Han et al. (2014a), near-surface Indian Ocean warming has been associated with anthropogenic greenhouse gases (e.g., Gregory et al. 2009; Gleckler et al. 2012, and references therein) through changes in downward longwave radiation and weakened winds suppressing turbulent heat loss from the ocean (Du and Xie 2008). However, the weakened winds and changes in heat loss are inconsistent with observed wind and heat flux trends (Yu and Weller 2007). The heat flux dilemma led Schott et al. (2009) to conclude that ocean dynamics must be playing a role in determining upper-ocean temperature trends in the Indian Ocean.

It was also noted that top 700-m Indian Ocean heat content did not increase during the second half of the twentieth century (Schott et al. 2009), a signal distinct from other (tropical) ocean basins (e.g., Balmaseda et al. 2013). Investigating temperature trends above 1000 m in the Indian Ocean thermal archive and climate models for the period 1960–99, Alory et al. (2007) found pronounced warming in the subtropical Indian Ocean 40°–50°S extending down to 800 m and attributed this to a southward shift in the subtropical gyre as a result of strengthening westerlies. A concurrent Indian Ocean subsurface cooling in the tropics was associated with

more frequent negative Indian Ocean dipole (IOD) events and a strengthened subtropical cell (Trenary and Han 2008), as well as a shoaling thermocline (Han et al. 2006; Cai et al. 2008) in response to changing Pacific wind forcing (Alory et al. 2007; Schwarzkopf and Böning 2011). The leading mode of upper-ocean Indo-Pacific temperatures in the Simple Ocean Data Assimilation product was also found to exhibit a long-term trend of surface warming and subsurface cooling at thermocline depth, which Vargas-Hernandez et al. (2014, 2015) linked to Pacific modes of climate variability, such as the IPO, North Pacific Gyre, and El Niño Modoki. Using sensitivity experiments with an OGCM, Schwarzkopf and Böning (2011) found the Indian Ocean subsurface cooling trend to be reproduced in simulations with observed wind forcing in the Pacific only, while wind stress outside the Pacific was kept at climatology. This highlights the role of remote Pacific wind forcing for upper-ocean temperature changes in the Indian Ocean.

It is well known that signals from remote Pacific wind forcing can be transmitted through the ITF region and result in thermocline depth and sea level variations along Western Australia, linked through coastal wave dynamics (Clarke and Liu 1994; Meyers 1996; Wijffels and Meyers 2004; Ummenhofer et al. 2013; Sprintall et al. 2014). On interannual time scales, El Niño–Southern Oscillation (ENSO) is the dominant driver, with the remote signal initiated by zonal wind anomalies in the central Pacific and transmitted by westward-propagating Rossby waves in the Pacific, becoming coastally trapped waves at the intersection of the equator and New Guinea (Wijffels and Meyers 2004). Along the Australian coastline, they travel poleward and radiate Rossby waves into the southern Indian Ocean (e.g., Cai et al. 2005). Shi et al. (2007) found the energy transmission from the Pacific to the Indian Ocean during ENSO events to be stronger after 1980 than before. Trenary and Han (2013) used OGCM experiments to assess the relative role of local Indian Ocean versus remote Pacific forcing on subsurface south Indian Ocean decadal variability. Focusing on decadal thermocline variations in the latitude range of 5°–17°S, they found these to be dominated by Ekman pumping through wind stress curl variations over the southern Indian Ocean. However, from the 1990s onward, these thermocline variations were primarily driven by changes in the Pacific trade winds (Trenary and Han 2013).

Equatorial zonal easterlies in the Pacific have been strengthening since the late 1990s associated with a negative IPO phase (England et al. 2014). Trends in Pacific equatorial wind stress can directly impact Indian Ocean upper-ocean thermal properties, transmitted through the ITF. The ITF transport has been strengthening at

1 Sv decade^{-1} (1 Sv $\equiv 10^6 \, \text{m}^3 \, \text{s}^{-1}$) during 1984–2013 according to a 30-yr expendable bathythermograph record between Fremantle in Western Australia and Sunda Strait, Indonesia (Liu et al. 2015). Using an 18-yr ITF proxy transport time series, developed from in situ measurements and altimetry, Sprintall and Revelard (2014) found significant increases in volume transport in the upper layer of Lombok Strait and over the full depth in Timor Passage since the early 1990s. This was also reflected in OGCM hindcast simulations in higher transport of the ITF and Leeuwin Current along the west coast of Australia post-1993 (Feng et al. 2011). More frequent Ningaloo Niño events (Feng et al. 2013), characterized by anomalously warm ocean conditions off Western Australia, were seen since the 1990s when positive heat content anomalies and cyclonic wind anomalies off Western Australia favored increased southward heat transport by the Leeuwin Current and were often preconditioned by SST in the far-western Pacific (Marshall et al. 2015). In addition to the well-known equatorial pathway transmitted through coastal wave dynamics through the ITF region, a pathway from the subtropical North Pacific was also proposed (Cai et al. 2005). However, it is unknown how the strength of this Pacific–Indian Ocean transmission varies on longer multidecadal time scales (Shi et al. 2007).

Changes in the eastern Indian Ocean background state on decadal time scales in turn have the potential to impact the leading mode of interannual variability in the Indian Ocean, the IOD (Saji et al. 1999; Webster et al. 1999). Annamalai et al. (2005) proposed that an altered background state of the eastern Indian Ocean thermocline on decadal time scales could precondition decades for strong positive IOD events. Investigating the rare occurrence of three consecutive positive IOD events observed in 2006–08 (Cai et al. 2009c), Cai et al. (2009d) proposed an anthropogenic contribution, as positive IOD events became more frequent over the period 1950–99 in climate models. This was considered consistent with a weaker Walker circulation over the Pacific and changing land–sea temperature gradients over the Indian Ocean. However, subsurface ocean conditions were found to be key for the development (and prediction) of the rare IOD events in 2006–08, with the triggering mechanism for such an event lying in the ocean (Cai et al. 2009c). It remains unclear, though, what role multidecadal variability plays in low-frequency changes in the occurrence of both positive and negative IOD events. On interannual time scales, Indian Ocean SST linked to the IOD has been found to impact regional climate in Indian Ocean rim countries (e.g., Webster et al. 1999; Abram et al. 2003; Ashok et al. 2003, 2004; Cai et al. 2009a,b; Ummenhofer et al. 2009b,c,

2011; D'Arrigo et al. 2011; García-García et al. 2011). Given the IOD's importance for regional climate in vulnerable societies in Indian Ocean rim countries, it is important to better understand how slowly evolving upper-ocean thermal properties on multidecadal time scales could precondition IOD events.

Here, we use hindcasts with a high-resolution OGCM to characterize multidecadal variations in the upper-ocean thermal structure of the Indian Ocean. Focus is on two specific objectives: 1) to examine the nature and origin of the low-frequency evolution of subsurface temperatures in the Indian Ocean and 2) to investigate the implications of these low-frequency thermal variations in the Indian Ocean for the IOD.

2. Data and methods

a. Datasets

A series of monthly global gridded observational and reanalysis products were used to assess decadal variability in thermal properties across the Indian and Pacific Oceans. At 1° horizontal resolution this includes the EN4.0.2 product by the Met Office (1900–present; Good et al. 2013), which uses quality-controlled subsurface ocean temperature and salinity profiles and objective analyses to also provide uncertainty estimates. The Ocean Reanalysis System 4 (ORAS4; 1958–present; Balmaseda et al. 2013) by the European Centre for Medium-Range Weather Forecasts (ECMWF) uses a sophisticated data assimilation methodology that includes a model bias correction to estimate the state of the global ocean via the operational system Ocean-S4. The ocean model is forced by atmospheric daily surface fluxes, relaxed to SST and bias corrected (National Center for Atmospheric Research 2014). The Pacific decadal oscillation (PDO) time series used consists of standardized values derived as the leading principal component of monthly SST anomalies in the North Pacific north of 20°N following Mantua et al. (1997).

b. Ocean model simulations

A series of global OGCM simulations was analyzed, building on an ocean–sea ice model. ORCA025 is an established eddy-active configuration at 0.25° nominal resolution (Barnier et al. 2006) based on the Nucleus for European Modelling of the Ocean (NEMO, version 3.1.1; Madec 2008). The effective resolution in the Indian Ocean varies between 21 and 28 km in the Indian Ocean, resolving the mesoscale equatorward of about 30°N and 30°S (Hallberg 2013). In the vertical, the model is discretized with 46 height (z) levels, starting with 10 levels in the upper 100 m and increasing to a thickness of

250 m at depth. The bottom grid cells are allowed to be partially filled, which in combination with an advanced advection scheme results in an improved global circulation (Barnier et al. 2006). Mixed layer dynamics and the vertical mixing are parameterized according to a turbulent kinetic energy scheme (Blanke and Delecluse 1993); lateral mixing is rotated and performed on isopycnals.

The model starts from initial conditions, with temperatures and salinities being initialized from a compilation of different observational datasets, in the Indian Ocean taken from the Levitus et al. (1998) climatology. For atmospheric forcing conditions of wind and thermohaline fluxes, we used the Large and Yeager (2009) dataset, which is originally based on the National Centers for Environmental Prediction (NCEP)–National Center for Atmospheric Research (NCAR) reanalysis products and corrected and globally balanced using various observational datasets. The forcing fields are provided at 6-hourly (wind, air temperature, and humidity), daily (shortwave and longwave radiation), and monthly (precipitation and runoff) resolution and applied through bulk formulas according to the Coordinated Ocean–Ice Reference Experiment phase 2 (CORE-II) protocol (Griffies et al. 2009). The ocean model is spun up over the period 1978–2007; based on this, the hindcast integration was performed over the full period 1948–2007.

The simulations used very weak sea surface salinity restoring at a 1-yr time scale (Behrens et al. 2013). This aspect is of particular importance in the context of this study for an almost free evolution of surface quantities. To identify and correct for spurious model drift, the simulation was repeated with global climatological (the "normal year" CORE product) forcing. The linear trends for the period 1952–2007 in the climatological simulation were subtracted from all interannually forced simulations. The trends in the climatological simulation are typically almost an order of magnitude smaller than the long-term trends in the simulations using interannual forcing.

3. Temperature trends in ocean reanalysis and hindcast

To assess the representation of Indian Ocean subsurface thermal properties in the ocean model, the linear trend in our hindcast is compared with the ORAS4 product for 1960–99, an analysis period used in previous studies (e.g., Alory et al. 2007; Alory and Meyers 2009; Schwarzkopf and Böning 2011). The linear trend of the Indian Ocean zonal mean temperature for the top 700 m reveals surface warming on the order of $0.02°C\ yr^{-1}$ in

the top 50 m across the Indian Ocean, extending deeper to 100–200 m south of 20°S in both ORAS4 and the ORCA hindcast (Figs. 1a,b). Also apparent is a strong subsurface cooling signal at 60–400-m depth for 8°–15°S; this subsurface cooling is stronger in the ORCA hindcast ($0.03°–0.06°C\ yr^{-1}$) than in ORAS4 (Figs. 1a,b). This prominent tropical subsurface cooling was found in previous observational and model-based studies (e.g., Han et al. 2006; Alory et al. 2007; Cai et al. 2008; Trenary and Han 2008; Schwarzkopf and Böning 2011) and proposed to be partially linked to changing (Pacific) wind forcing.

As can be seen here exemplarily for the 190-m depth level for both ORAS4 and ORCA (Figs. 1c,d), the subsurface cooling trend centers at 12°S and extends across the entire tropical Indian Ocean. The spatial pattern of the tropical subsurface cooling trend compares well between ORAS4 and ORCA, both across the Indian Ocean and for the extensive cooling seen in the Pacific over 20°N–10°S. Also apparent is the warming in the southern Indian Ocean, centered at 30°S (Figs. 1c,d) that has previously been associated with a southward shift of the subtropical gyre (Alory et al. 2007).

Zonal cross sections of the temperature trend centered along the equator and along 10°S further highlight the associated depth structure (Figs. 1e–h): strong warming in excess of $0.025°C\ yr^{-1}$ is restricted to a thin surface layer extending to 100-m (less than 50 m) depth along the equator (at 10°S); the surface warming trend in the eastern equatorial Indian Ocean is stronger in ORAS4 than in our ORCA hindcast (Figs. 1e,f). The strong subsurface cooling in excess of $0.1°C\ yr^{-1}$ is especially prominent in the 10°S cross section, extending over the 60–400-m depth range and across the entire width of the Indian Ocean (Figs. 1g,h). For the equatorial cross section, the subsurface cooling in the ORCA hindcast is limited to the 100–320-m depth range in the western Indian Ocean and somewhat narrower in the east, while it extends below 400 m in the west (300 m in the east) in ORAS4 (Figs. 1e,f).

Overall, the spatial patterns of multidecadal Indian Ocean (subsurface) temperature trends in our ORCA simulations compare well with the trends in the ORAS4 product. Caution needs to be used when analyzing trends in the observational-based EN4 product in data-sparse regions, as the objectively analyzed EN4 gridded temperature in the absence of any observations is relaxed to the 1971–2000 climatology (Good et al. 2013). With this caveat in mind and especially relevant in the data-sparse Indian Ocean, subsurface temperature trends in the ORCA simulations across the Indian Ocean are also in broad agreement with the subsurface temperature trends, albeit weak and patchy, in the
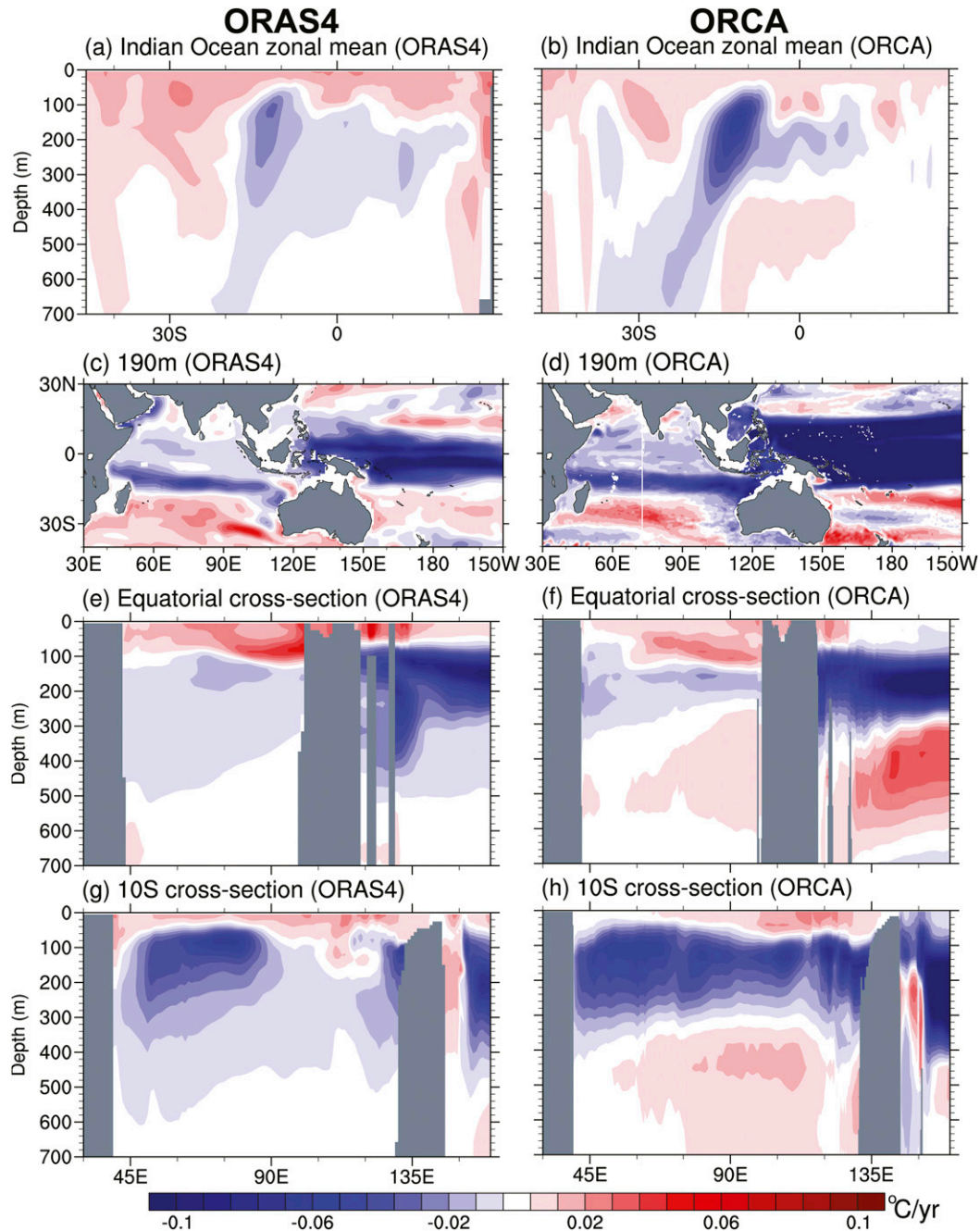
FIG. 1. Temperature trends (°C yr⁻¹) for the period 1960–99 for (left) ORAS4 and (right) ORCA hindcast: (a),(b) Indian Ocean zonal mean temperature, (c),(d) temperature at 190-m depth, and (e)–(h) zonal cross sections along the (e),(f) equator and (g),(h) 10°S.

observational-based EN4 product (figure not shown). This gives us confidence that the OGCM hindcast exhibits sufficient skill in representing low-frequency upper-ocean thermal variations across the Indo-Pacific for the present work. Previous studies have also used ORCA simulations for understanding links between Pacific forcing and Indian Ocean variability on interannual (Ummenhofer et al. 2013) and decadal (Schwarzkopf and Böning 2011) time scales; they provide further details on the model's representation of Indo-Pacific upper-ocean variability.

In light of these striking upper-ocean temperature trends in the Indian Ocean, it is of interest to explore the temporal evolution of subsurface heat content in the

Indo-Pacific. In particular, we are interested in better understanding how these well-described long-term trends relate to the evolution of the upper-ocean thermal structure of the Indian Ocean on multi-decadal time scales. Ocean model hindcasts represent a tool well suited to this endeavor because they are based on a dynamically consistent framework, allow for an almost free evolution of ocean surface quantities, and do not employ infilling of missing data based on climatology for a subset of decades. The latter makes observational or ocean reanalysis products that relax to climatology in the absence of observations (Good et al. 2013) or use data assimilation (Stammer et al. 2016) problematic for trend analysis on multidecadal time scales and beyond. However, comparing Indian Ocean mean temperature trends in the 1990s and 2000s based on various observational-based products and ocean reanalyses, Nieves et al. (2015) found ORAS4 temperature trends in the top 400 m to be consistent with those obtained from the *World Ocean Atlas* (*WOA*; Levitus et al. 2012) and the Ishii dataset (Ishii et al. 2005), while several other reanalysis products exhibited diverging trends. Agreement between ORAS4 and the *WOA* and Ishii dataset below 500 m was reduced (Nieves et al. 2015). Consequently, and as a result of the apparent disagreement in the temperature trend below 400 m in parts of the Indian Ocean between ORAS4 and the ORCA simulations (cf. Figs. 1e,f), we focus our following analyses on the 100–320-m depth range.

4. Temporal evolution of Indian Ocean heat content and links to the Pacific

Subsurface heat content anomalies for 8-yr intervals were calculated as the integrated temperature for the depth range 100–320 m relative to the analysis period 1952–2007 (Fig. 2). The period 1952–59 was characterized by warm heat content anomalies in the western and central Pacific (15°S–30°N; Fig. 2a). The Indonesian–Australian Basin extending toward the central Indian Ocean exhibited warm heat content anomalies in the 1950s, but over the 1960s warm heat content anomalies extended westward across much of the Indian Ocean (0°–20°S; Figs. 2a,b). Over the period 1968–75, warm anomalies weakened in the western Pacific and across the Indian Ocean (Fig. 2c). From 1976 onward, cool heat content anomalies appeared in the western Pacific, intensifying over the 1980s (Figs. 2d,e). By the early 1990s, cool heat content anomalies expanded north-westward from the eastern Indian Ocean (10°–30°S, 80°–120°E), reaching the western Indian Ocean in the 2000s (Figs. 2e–g).
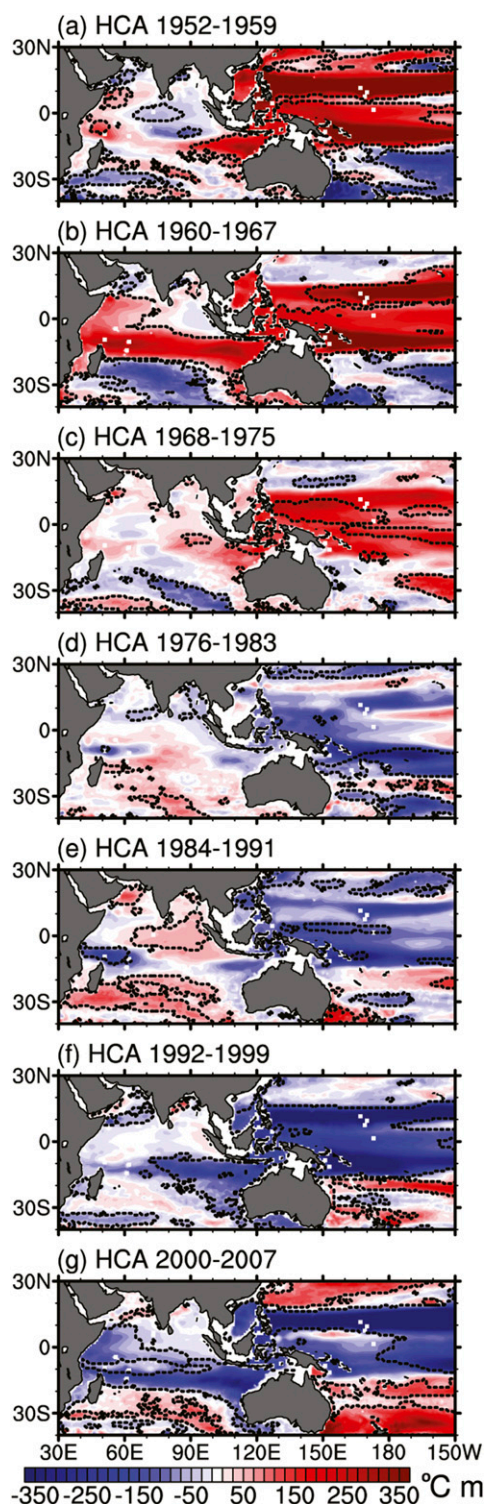

FIG. 2. Subsurface heat content anomaly (°C m) in the 100–320-m depth range and averaged for 8-yr intervals relative to the analysis period 1952–2007 in the ocean model hindcast. The area enclosed by dashed contours denotes anomalies significant at the 90% level as estimated by the two-tailed Student's *t* test.

The westward expansion of anomalous high sub-surface heat content in the 1960s and 1970s across the Indian Ocean is also apparent in a longitude–time Hovmöller plot (Fig. 3). After the 1990s, cooler anomalies in heat content similarly expanded westward across the Indian Ocean (Fig. 3). The spatial pattern of the westward expansion/spreading of the heat content anomaly in the Indian Ocean is reminiscent to the one described by Ummenhofer et al. (2013) on interannual time scales. This was associated with Rossby waves radiating into the southern Indian Ocean, transmitting the ENSO signal to the Indian Ocean, as detected in variations in the depth of the 20°C isotherm for example (Cai et al. 2005). On interannual time scales, Xie et al. (2002) found southwest Indian Ocean thermocline variance to be highly correlated with eastern Pacific SST conditions at a lag of 3 months, transmitted through downwelling Rossby waves propagating westward at a phase speed of 35° longitude yr^{-1} in the latitude range of 8°–12°S in the Indian Ocean. Westward-propagating baroclinic Rossby waves play an important role in the southern Indian Ocean circulation in the latitude range of 8°–15°S (e.g., Masumoto and Meyers 1998; Jury and Huang 2004; Baquero-Bernal and Latif 2005; Chowdary et al. 2009; Schott et al. 2009). Furthermore, the Indian Ocean's South Equatorial Current distributes ITF waters across the Indian Ocean, with the bulk of the transport occurring within the thermocline layer (Gordon et al. 1997, and references therein). Observed ITF transport based on expendable bathythermograph (XBT) lines, in situ measurements, and altimetry has increased since the 1980s (Liu et al. 2015) and early 1990s (Sprintall and Revelard 2014). While enhanced ITF transport is consistent with recent subsurface warming trends in the Indian Ocean since the late 1990s (Lee et al. 2015; Nieves et al. 2015), these ITF trends cannot account for the long-term subsurface cooling trend centered near 10°S seen for the 1960s–late 1990s. This is despite the fact that ORCA hindcast simulations also detected higher transport of the ITF and Leeuwin Current along Western Australia after 1993 (Feng et al. 2011).

Instead, the response of subsurface heat content anomalies in the Indian Ocean to remote Pacific variations on the decadal and/or multidecadal time scales shown here (Fig. 2) is reminiscent of a thermocline response to Rossby wave propagation, as seen on interannual time scales (Ummenhofer et al. 2013). As such, the Indian Ocean subsurface heat content change appears to be a low-frequency adjustment of the thermocline in response to Pacific forcing. It is reminiscent of the well-known adjustment of the western Pacific thermocline depth (Collins et al. 2010; Williams and
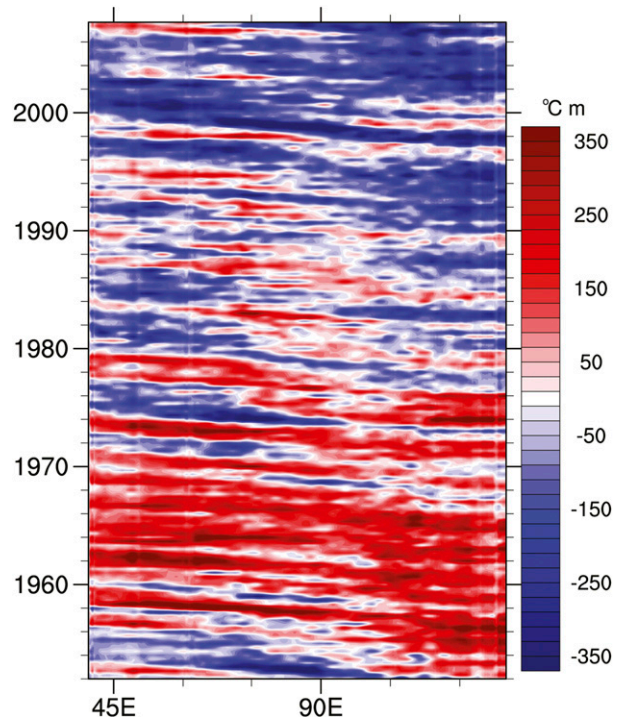

FIG. 3. Hovmöller plot of subsurface heat content anomaly (°C m) in the 100–320-m depth range across the Indian Ocean averaged for the 7°–15°S latitude range in the ocean model hindcast.

Grottoli 2010) to equatorial wind stress forcing in the Pacific on decadal time scales (Schwarzkopf and Böning 2011). In a similar vein, using an OGCM hindcast and multicentury climate model simulations, Shi et al. (2007) proposed a multidecadal variation in the strength of the transmission of the ENSO-associated Rossby wave signal to the Indian Ocean but found it hard to detect the transmission signal during weak-ENSO periods.

To better evaluate the low-frequency evolution of these Indian Ocean subsurface temperature variations, Fig. 4a shows the time series of zonal mean Indian Ocean (IO) subsurface (100–320 m) temperature for the 5°–15°S latitude band. The time series is characterized by a warm phase extending from the mid-1950s to the mid-1970s (IO phase A), followed by a transition period in the late 1970s, and a cool phase from the 1980s onward (IO phase B). The change in the Indian Ocean zonal mean subsurface temperature is on the order of from +0.6° to +0.8°C in the high phase to −0.6°C in the cool phase (Fig. 4a), a considerable temperature change in light of the areal extent. This is also reflected in a substantial change in Indian Ocean heat content: during IO phase A, high heat content anomalies dominated for much of the tropical Indian Ocean north of 15°S, coincident with extensive high anomalies across the Pacific (15°S–20°N; Fig. 4c). In contrast, IO phase B exhibited
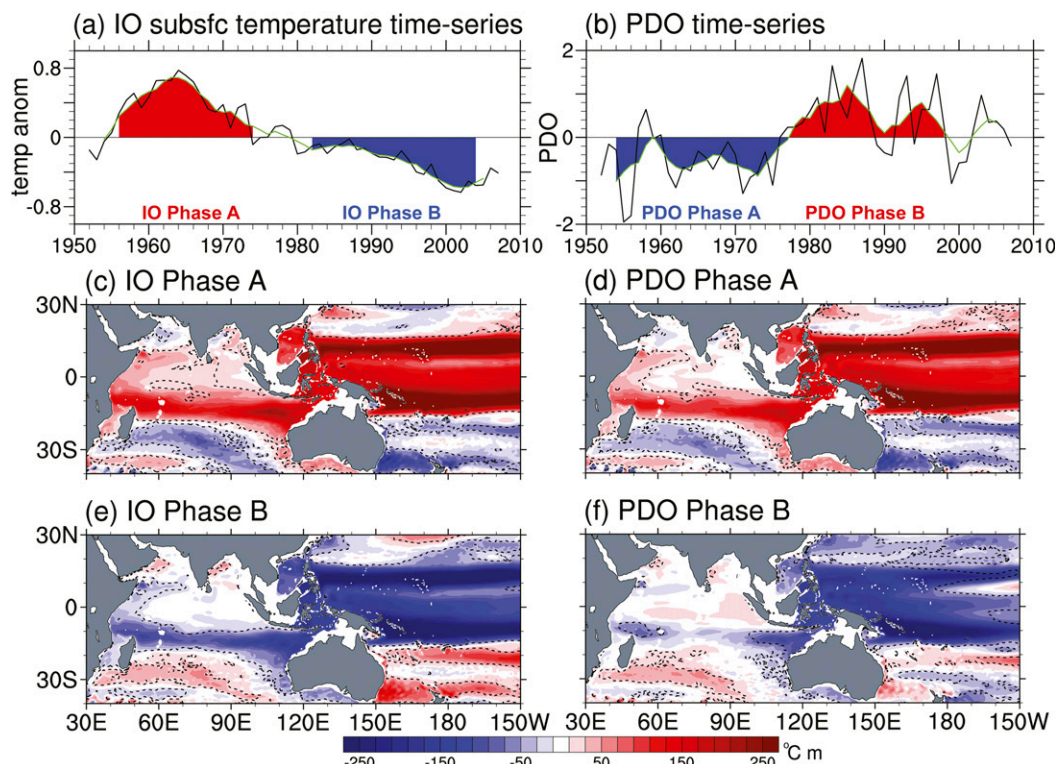
FIG. 4. Time series of (a) Indian Ocean subsurface zonal mean temperature (5°–15°S) and (b) PDO. The green line represents a 5-yr running mean. Composites of subsurface heat content anomaly (°C m) in the 100–320-m depth range during years in the phases highlighted in the time series for (c),(e) low-frequency Indian Ocean subsurface temperature variations and (d),(f) in the PDO. The area enclosed by dashed contours denotes anomalies significant at the 90% level as estimated by the two-tailed Student's t test.

cool heat content anomalies in a latitudinal band extending from the eastern Indian Ocean along 5°–15°S to the west and across the tropical–subtropical Pacific (Fig. 4e).

Given the extensive Pacific Ocean heat content signals seen in the analyses so far (Figs. 2 and 4c,e), it is of interest to relate Indian Ocean heat content to low-frequency Pacific variability, namely the PDO. The PDO time series indicates its prominent cool and warm phases in the 1960s–1970s and the 1980s–1990s, respectively (Fig. 4b). Indo-Pacific heat content anomalies during PDO phase A were very similar to those during IO phase A (Figs. 4c,d), consistent with the large overlap in the periods. In contrast, PDO phase B (1979–98) exhibited extensive cool heat content anomalies across the Pacific, but only in a small area in the eastern Indian Ocean off the northwestern shelf of Australia (Fig. 4f). Spreading of cool heat content anomalies across the Indian Ocean, as seen during IO phase B (1982–2004), was only starting in PDO phase B (Figs. 4e,f). Over the full analysis period of 1952–2007, the Indian Ocean subsurface temperature is significantly correlated at a

5–6-yr lag with the PDO index (Pearson correlation coefficient of 0.45; $P > 0.001$) and western Pacific subsurface temperature for the depth range 100–320 m in the 0°–12°N, 135°–150°E region (correlation coefficient of 0.59; $P > 0.001$).

As summarized in a review by Newman et al. (2016), North Pacific variability associated with the PDO impacts tropical Pacific variability through variations in the subtropical winds. These in turn modulate the strength of the overturning circulation in the subtropical cells (STCs) in the Pacific, affecting the southward advection of relatively cold extratropical waters, which—through equatorial upwelling—drive air–sea feedbacks and thus decadal variability in the tropics. Using observations of the 25.0 kg m^{-3} potential density surface as a measure of the upper pycnocline, McPhaden and Zhang (2002) showed a slowdown in the STC between the early 1970s and late 1990s, with a transit time of 5–10 yr to transmit a signal from the North Pacific to the equator. Depth differences of 25–30 m in the western equatorial Pacific upper pycnocline between these two time periods in McPhaden and Zhang (2002), which they tentatively
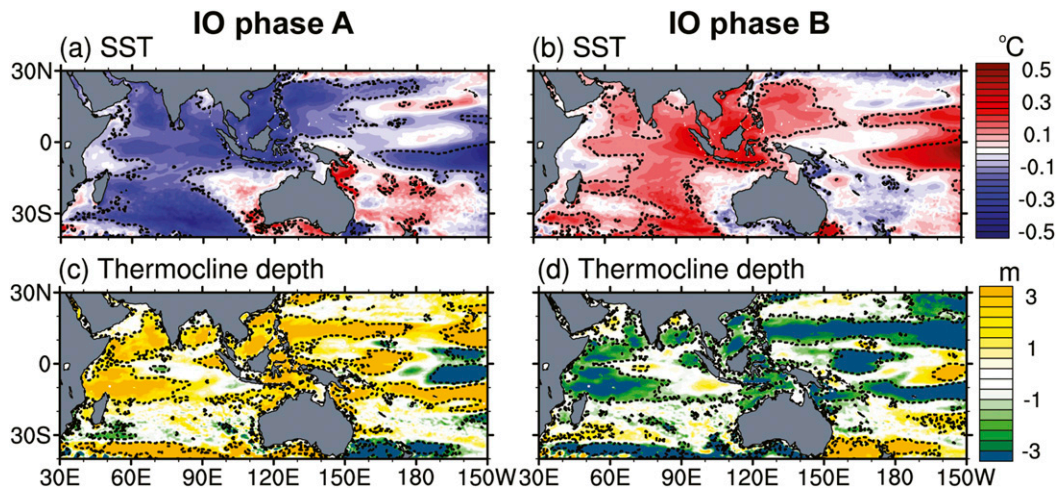
FIG. 5. Composite anomaly during years in (left) phase A and (right) phase B for low-frequency Indian Ocean subsurface temperature variations (cf. periods highlighted in Fig. 4a) for (a),(b) SST (°C) and (c),(d) thermocline depth (m). The area enclosed by dashed contours denotes anomalies significant at the 90% level as estimated by the two-tailed Student's *t* test.

linked to the PDO, exhibit spatial patterns reminiscent of the western Pacific heat content anomalies shown here (Fig. 2). Several other previous studies also related subsurface temperatures, sea surface height, and sea level variations in the western Pacific that can be affected by the PDO to (south)eastern Indian Ocean on decadal time scales (e.g., Lee and McPhaden 2008; Schwarzkopf and Böning 2011; Nidheesh et al. 2013; Vargas-Hernandez et al. 2014), with the relationship strengthening in recent decades (Trenary and Han 2013; Han et al. 2014b; Feng et al. 2015).

5. Links between Indian Ocean subsurface temperature variations and IOD events

It is important to ascertain how the different Indian Ocean background state in subsurface heat content relates to upper-ocean properties with relevance to surface expressions. Composite anomalies of SST and thermocline depth during the two different phases (i.e., IO phases A and B identified in Fig. 4) are shown in Fig. 5. The thermocline depth here is taken as the depth corresponding to the base of the mixed layer, which is water with differences in potential density of less than $0.01 \, kg \, m^{-3}$. IO phase A (1956–74) was characterized by anomalously cool SST in excess of $-0.5°C$ over much of the tropical and subtropical Indian Ocean, with the exception of the far-southeastern Indian Ocean along the Western Australia coast and the northwestern shelf of Australia (Fig. 5a). At the same time, the thermocline was anomalously deep, especially over the northwestern shelf of Australia and in the western Indian Ocean, with

anomalies in excess of $+3 \, m$ (Fig. 5c). In contrast, IO phase B (1982–2004) exhibited anomalously warm SST in excess of $+0.5°C$ in the central tropical and subtropical Indian Ocean and a shallower thermocline depth in the western Indian Ocean and the ITF region (Figs. 5c,d).

It has been proposed that the background state of the eastern Indian Ocean thermocline depth can modulate the frequency of occurrence of IOD events on decadal time scales (Annamalai et al. 2005). The time series of eastern Indian Ocean (0°–10°S, 90°–110°E) thermocline depth reflects interannual variations in excess of $\pm 6 \, m$, superimposed on low-frequency variations in the background state of $\pm 2 \, m$ for a decade or more (blue and red shaded periods in Fig. 6a). The numbers of positive IOD (pIOD) and negative IOD (nIOD) events also exhibit low-frequency variations.

To determine whether the frequency of pIOD and nIOD events during periods with a deep or shallow eastern Indian Ocean thermocline were unusual, a bootstrapping technique was used to generate an expected distribution based on random events using all years. The box-and-whisker plots in Fig. 6b summarize these expected distributions for pIOD and nIOD, respectively. Given the uneven number of pIOD and nIOD events, the expected distributions for the two phases can differ. The same applies to the number of years with a deep or shallow thermocline background state. From the bootstrapping method, each actual event also has an error bar associated with it. Where the error bar of the actual event does not overlap with the associated box and whisker of the expected distribution, the
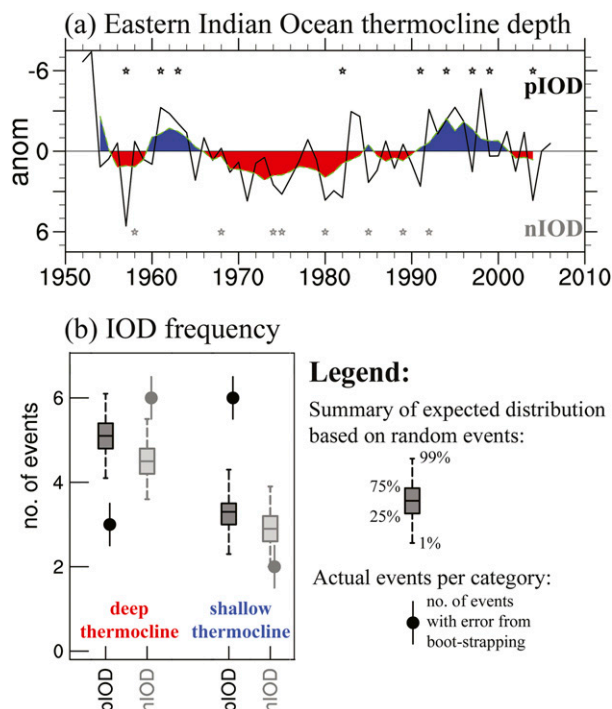
FIG. 6. (a) Time series of eastern Indian Ocean thermocline depth for annual values (black) and a 5-yr running average (green). With the y axis inverted, positive anomalies reflect a deepening (red) and negative anomalies a shallowing (blue) of the thermocline depth; pIOD and nIOD years [according to Ummenhofer et al. (2009a)] are marked by black and gray stars, respectively. (b) Circles (with corresponding bootstrapped error bars) indicate the actual number of IOD events that occur during periods with anomalously deep or shallow thermocline depth. To determine whether the event frequency of pIOD and nIOD is unusual, a bootstrapping technique is used to generate an expected distribution based on random events using all years. The box-and-whisker plot summarizes this expected distribution. Where the error bar of the actual event does not overlap with its associated expected distribution in the box-and-whisker plot the number of events is significantly different from a sample based on all years at the 98% level.

number of events is significantly different from a sample based on all years at the 98% level.

During periods with a deep thermocline background state in the 1970s and 1980s, pIOD events were unusually rare with only 3 ($\pm$0.5) events, while 6 ($\pm$0.5) nIOD events occurred (Fig. 6b). In contrast, when the eastern Indian Ocean thermocline depth was in a shallow state, such as in the 1960s and 1990s, pIOD events were significantly more common with 6 ($\pm$0.5) events. Given that the eastern Indian Ocean in its climatological state is characterized by relatively warm SST and a deep thermocline compared to the Pacific and Atlantic (Jansen et al. 2009), a shallower thermocline favored the development of positive Bjerknes-type feedback and

allowed for more frequent pIOD events; the number of nIOD events on the other hand was not affected (Fig. 6b). A deepening of the thermocline reinforces the climatological background state, further hampering the development of a positive feedback in thermocline–SST coupling over the eastern Indian Ocean; this was reflected in a lower number of pIOD events, while nIOD events were more common. Decadal variations in Indian Ocean SST associated with the IOD have previously been linked to the PDO and IPO (Annamalai et al. 2005; Han et al. 2014b; Dong et al. 2016; Krishnamurthy and Krishnamurthy 2016). Using partial coupling experiments with the Community Climate System Model, version 4, Krishnamurthy and Krishnamurthy (2016) proposed a link from the North Pacific to the Indian Ocean excited by northerly wind variations in the western North Pacific.

6. Conclusions

The Indian Ocean has sustained robust surface warming in the second half of the twentieth century, accompanied by strong tropical subsurface cooling in excess of 0.1°C yr^{-1} especially prominent near 10°S, extending over the 60–400-m depth range and across the entire width of the Indian Ocean. These spatial patterns of Indian Ocean (subsurface) temperature trends were well reproduced in the OGCM simulations in this study, when compared to trends in observational and reanalysis products.

Previous work focused on diagnosing the thermal structure and cause of these long-term trends in Indian Ocean temperatures in the top 500 m over the second half of the twentieth century. Here, we instead interpret these trends to result from aliasing of the considerable multidecadal variations that exist in upper-ocean heat content in the Indian Ocean and can be linked to broader Indo-Pacific low-frequency variability: the 1950s were characterized by warm heat content anomalies in the western and central Pacific. In the Indian Ocean, the Indonesian–Australian Basin extending toward the central Indian Ocean exhibited warm heat content anomalies in the 1950s, but over the 1960s warm heat content anomalies extended westward across much of the Indian Ocean (0°–20°S). From 1976 onward, cool anomalies appeared in the western Pacific, intensifying over the 1980s. By the early 1990s, cool anomalies expanded northwestward from the eastern Indian Ocean, reaching the western Indian Ocean in the 2000s. To better evaluate the low-frequency evolution of these Indian Ocean subsurface temperature variations, we determined a warm phase extending from the mid-1950s to the mid-1970s, followed by a transition period in the late 1970s and a cool phase from the 1980s onward. These related to low-frequency Pacific variability, namely

the PDO; lead–lag relationships between Indian Ocean subsurface temperatures revealed a multiyear lag with the PDO and western Pacific subsurface temperatures at 5–6 yr, potentially mediated through an adjustment of the STC and equatorial upwelling in the Pacific (McPhaden and Zhang 2002).

Variations in subsurface heat content coincide with changes in the thermocline depth over the eastern Indian Ocean. Changes in the background state of the eastern Indian Ocean thermocline have been proposed to modulate the frequency of occurrence of strong positive IOD events on decadal time scales (Annamalai et al. 2005). The eastern Indian Ocean thermocline depth in our hindcast simulations here indeed reflected considerable low-frequency variations. The numbers of pIOD and nIOD events also exhibited low-frequency variations; pIOD events occurred significantly more (less) frequently during periods with a shallow (deep) thermocline, while nIOD events were more common when the thermocline was deep. Our results demonstrate that changes in the background state of the subsurface Indian Ocean affect the dominant mode of Indian Ocean interannual variability (i.e., IOD). Our results also have implications for decadal predictions. In fact, the Indian Ocean stands out as the region globally where SST state-of-the-art decadal climate predictions for the 2–9-yr range perform best (Guemas et al. 2013). They attribute this to the Indian Ocean being the region with the lowest ratio of internally generated over externally forced variability, which is consistent with our findings here.

REFERENCES

Abram, N. J., M. K. Gagan, M. T. McCulloch, J. Chappell, and W. S. Hantoro, 2003: Coral reef death during the 1997 Indian Ocean dipole linked to Indonesian wildfires. *Science*, **301**, 952–955, doi:10.1126/science.1083841.

Alory, G., and G. Meyers, 2009: Warming of the upper equatorial Indian Ocean and changes in the heat budget (1960–99). *J. Climate*, **22**, 93–113, doi:10.1175/2008JCLI2330.1.

——, S. Wijffels, and G. Meyers, 2007: Observed temperature trends in the Indian Ocean over 1960–1999 and associated mechanisms. *Geophys. Res. Lett.,* **34**, L02606, doi:10.1029/2006GL028044.

Annamalai, H., J. Potemra, R. Murtugudde, and J. P. McCreary, 2005: Effect of preconditioning on the extreme climate events in the tropical Indian Ocean. *J. Climate*, **18**, 3450–3469, doi:10.1175/JCLI3494.1.

Ashok, K., Z. Guan, and T. Yamagata, 2003: Influence of the Indian Ocean dipole on the Australian winter rainfall. *Geophys. Res. Lett.*, **30**, 1821, doi:10.1029/2003GL017926.

——, ——, N. H. Saji, and T. Yamagata, 2004: Individual and combined influences of the ENSO and Indian Ocean dipole on the Indian summer monsoon. *J. Climate*, **17**, 3141–3155, doi:10.1175/1520-0442(2004)017<3141:IACIOE>2.0.CO;2.

Balmaseda, M. A., K. Mogensen, and A. T. Weaver, 2013: Evaluation of the ECMWF ocean reanalysis system ORAS4. *Quart. J. Roy. Meteor. Soc.*, **139**, 1132–1161, doi:10.1002/qj.2063.

Baquero-Bernal, A., and M. Latif, 2005: Wind-driven oceanic Rossby waves in the tropical South Indian Ocean with and without an active ENSO. *J. Phys. Oceanogr.*, **35**, 729–746, doi:10.1175/JPO2723.1.

Barnier, B., and Coauthors, 2006: Impact of partial steps and momentum advection schemes in a global ocean circulation model at eddy permitting resolution. *Ocean Dyn.*, **56**, 543–567, doi:10.1007/s10236-006-0082-1.

Behrens, E., A. Biastoch, and C. W. Böning, 2013: Spurious AMOC trends in global ocean sea-ice models related to subarctic freshwater forcing. *Ocean Modell.*, **69**, 39–49, doi:10.1016/j.ocemod.2013.05.004.

Blanke, B., and P. Delecluse, 1993: Variability of the tropical Atlantic Ocean simulated by a general circulation model with two different mixed-layer physics. *J. Phys. Oceanogr.*, **23**, 1363–1388, doi:10.1175/1520-0485(1993)023<1363:VOTTAO>2.0.CO;2.

Cai, W., G. Meyers, and G. Shi, 2005: Transmission of ENSO signal to the Indian Ocean. *Geophys. Res. Lett.*, **32**, L05616, doi:10.1029/2004GL021736.

——, A. Sullivan, and T. Cowan, 2008: Shoaling of the off-equatorial south Indian Ocean thermocline: Is it driven by anthropogenic forcing? *Geophys. Res. Lett.*, **35**, L12711, doi:10.1029/2008GL034174.

——, T. Cowan, and M. Raupach, 2009a: Positive Indian Ocean dipole events precondition southeast Australia bushfires. *Geophys. Res. Lett.*, **36**, L19710, doi:10.1029/2009GL039902.

——, ——, and A. Sullivan, 2009b: Recent unprecedented skewness towards positive Indian Ocean dipole occurrences and their impact on Australian rainfall. *Geophys. Res. Lett.*, **36**, L11705, doi:10.1029/2009GL037604.

——, A. Pan, D. Roemmich, T. Cowan, and X. Guo, 2009c: Argo profiles a rare occurrence of three consecutive positive Indian Ocean dipole events, 2006–2008. *Geophys. Res. Lett.*, **36**, L08701, doi:10.1029/2008GL037038.

——, A. Sullivan, and T. Cowan, 2009d: Climate change contributes to more frequent consecutive positive Indian Ocean dipole events. *Geophys. Res. Lett.*, **36**, L23704, doi:10.1029/2009GL040163.

Chowdary, J. S., C. Gnanaseelan, and S. P. Xie, 2009: Westward propagation of barrier layer formation in the 2006–07 Rossby wave event over the tropical southwest Indian Ocean. *Geophys. Res. Lett.*, **36**, L04607, doi:10.1029/2008GL036642.

Clarke, A. J., and X. Liu, 1994: Interannual sea level in the northern and eastern Indian Ocean. *J. Phys. Oceanogr.*,

24, 1224–1235, doi:10.1175/1520-0485(1994)024<1224:ISLITN>2.0.CO;2.

Collins, M., and Coauthors, 2010: The impact of global warming on the tropical Pacific and El Niño. *Nat. Geosci.*, **3**, 391–397, doi:10.1038/ngeo868.

D'Arrigo, R., N. Abram, C. Ummenhofer, J. Palmer, and M. Mudelsee, 2011: Reconstructed streamflow for Citarum River, Java, Indonesia: Linkages to tropical climate dynamics. *Climate Dyn.*, **36**, 451–462, doi:10.1007/s00382-009-0717-2.

Dong, L., T. Zhou, A. Dai, F. Song, B. Wu, and X. Chen, 2016: The footprint of the inter-decadal Pacific oscillation in Indian Ocean sea surface temperatures. *Sci. Rep.*, **6**, 21251, doi:10.1038/srep21251.

Du, Y., and S.-P. Xie, 2008: Role of atmospheric adjustments in the tropical Indian Ocean warming during the 20th century in climate models. *Geophys. Res. Lett.*, **35**, L08712, doi:10.1029/2008GL033631.

England, M. H., and Coauthors, 2014: Recent intensification of wind-driven circulation in the Pacific and the ongoing warming hiatus. *Nat. Climate Change*, **4**, 222–227, doi:10.1038/nclimate2106.

Feng, M., C. Böning, A. Biastoch, E. Behrens, E. Weller, and Y. Masumoto, 2011: The reversal of the multi-decadal trends of the equatorial Pacific easterly winds, and the Indonesian Throughflow and Leeuwin Current transports. *Geophys. Res. Lett.*, **38**, L11604, doi:10.1029/2011GL047291.

——, M. J. McPhaden, S.-P. Xie, and J. Hafner, 2013: La Niña forces unprecedented Leeuwin Current warming in 2011. *Sci. Rep.*, **3**, 1277, doi:10.1038/srep01277.

——, H. H. Hendon, S.-P. Xie, A. G. Marshall, A. Schiller, Y. Kosaka, N. Caputi, and A. Pearce, 2015: Decadal increase in Ningaloo Niño since the late 1990s. *Geophys. Res. Lett.*, **42**, 104–112, doi:10.1002/2014GL062509.

García-García, D., C. C. Ummenhofer, and V. Zlotnicki, 2011: Australian water mass variations from GRACE data linked to Indo-Pacific climate variability. *Remote Sens. Environ.*, **115**, 2175–2183, doi:10.1016/j.rse.2011.04.007.

Gleckler, P. J., and Coauthors, 2012: Human-induced global ocean warming on multidecadal timescales. *Nat. Climate Change*, **2**, 524–529, doi:10.1038/nclimate1553.

Good, S. A., M. J. Martin, and N. A. Rayner, 2013: EN4: Quality controlled ocean temperature and salinity profiles and monthly objective analyses with uncertainty estimates. *J. Geophys. Res. Oceans*, **118**, 6704–6716, doi:10.1002/2013JC009067.

Gordon, A. L., S. Ma, D. B. Olson, P. Hacker, A. Ffield, L. D. Talley, D. Wilson, and M. Baringer, 1997: Advection and diffusion of Indonesian Throughflow water within the Indian Ocean South Equatorial Current. *Geophys. Res. Lett.*, **24**, 2573–2576, doi:10.1029/97GL01061.

Gregory, J. M., H. T. Banks, P. A. Stott, J. A. Lowe, and M. D. Palmer, 2009: Simulated and observed decadal variability in ocean heat content. *Geophys. Res. Lett.*, **31**, L15312, doi:10.1029/2004GL020258.

Griffies, S. M., and Coauthors, 2009: Coordinated Ocean-ice Reference Experiments (COREs). *Ocean Modell.*, **26**, 1–46, doi:10.1016/j.ocemod.2008.08.007.

Guemas, V., S. Corti, J. Garcia-Serrano, F. J. Doblas-Reyes, M. Balmaseda, and L. Magnusson, 2013: The Indian Ocean: The region of highest skill worldwide in decadal climate prediction. *J. Climate*, **26**, 726–739, doi:10.1175/JCLI-D-12-00049.1.

Hallberg, R., 2013: Using a resolution function to regulate parameterizations of oceanic mesoscale eddy effects. *Ocean Modell.*, **72**, 92–103, doi:10.1016/j.ocemod.2013.08.007.

Han, W., G. A. Meehl, and A. Hu, 2006: Interpretation of tropical thermocline cooling in the Indian and Pacific Oceans during recent decades. *Geophys. Res. Lett.*, **33**, L23615, doi:10.1029/2006GL027982.

——, H. Vialard, M. J. McPhaden, T. Lee, Y. Masumoto, M. Feng, and W. P. M. de Ruijter, 2014a: Indian Ocean decadal variability: A review. *Bull. Amer. Meteor. Soc.*, **95**, 1679–1703, doi:10.1175/BAMS-D-13-00028.1.

——, and Coauthors, 2014b: Intensification of decadal and multidecadal sea level variability in the western tropical Pacific during recent decades. *Climate Dyn.*, **43**, 1357–1379, doi:10.1007/s00382-013-1951-1.

Ishii, M., A. Shouji, S. Sugimoto, and T. Matsumoto, 2005: Objective analyses of sea-surface temperature and marine meteorological variables for the 20th century using ICOADS and the Kobe collection. *Int. J. Climatol.*, **25**, 865–879, doi:10.1002/joc.1169.

Jansen, M. F., D. Dommenget, and N. Keenlyside, 2009: Tropical atmosphere–ocean interactions in a conceptual framework. *J. Climate*, **22**, 550–567, doi:10.1175/2008JCLI2243.1.

Jury, M. R., and B. Huang, 2004: The Rossby wave as a key mechanism of Indian Ocean climate variability. *Deep-Sea Res. I*, **51**, 2123–2136, doi:10.1016/j.dsr.2004.06.005.

Kosaka, Y., and S.-P. Xie, 2013: Recent global-warming hiatus tied to equatorial Pacific surface cooling. *Nature*, **501**, 403–407, doi:10.1038/nature12534.

Krishnamurthy, L., and V. Krishnamurthy, 2016: Decadal and interannual variability of the Indian Ocean SST. *Climate Dyn.*, **46**, 57–70, doi:10.1007/s00382-015-2568-3.

Large, W., and S. Yeager, 2009: The global climatology of an interannually varying air–sea flux data set. *Climate Dyn.*, **33**, 341–364, doi:10.1007/s00382-008-0441-3.

Lee, S.-K., W. Park, M. O. Baringer, A. L. Gordon, B. Huber, and Y. Liu, 2015: Pacific origin of the abrupt increase in Indian Ocean heat content during the warming hiatus. *Nat. Geosci.*, **8**, 445–450, doi:10.1038/ngeo2438.

Lee, T., and M. J. McPhaden, 2008: Decadal phase change in large-scale sea level and winds in the Indo-Pacific region at the end of the 20th century. *Geophys. Res. Lett.*, **35**, L01605, doi:10.1029/2007GL032419.

Levitus, S., and Coauthors, 1998: *World Ocean Database 1998*, volume 1: Introduction. NOAA Atlas NESDIS 18, 346 pp.

——, and Coauthors, 2012: World ocean heat content and thermosteric sea level change (0–2000 m), 1950–2010. *Geophys. Res. Lett.*, **39**, L10603, doi:10.1029/2012GL051106.

Liu, Q.-Y., M. Feng, D. Wang, and S. Wijffels, 2015: Interannual variability of the Indonesian Throughflow transport: A revisit based on 30-year expendable bathythermograph data. *J. Geophys. Res. Oceans*, **120**, 8270–8282, doi:10.1002/2015JC011351.

Madec, G., 2008: NEMO ocean engine, version 3.1. L'Institut Pierre-Simon Laplace Tech. Rep. 27, 27 pp.

Mantua, N. J., S. R. Hare, Y. Zhang, J. M. Wallace, and R. C. Francis, 1997: A Pacific interdecadal climate oscillation with impacts on salmon production. *Bull. Amer. Meteor. Soc.*, **78**, 1069–1079, doi:10.1175/1520-0477(1997)078<1069:APICOW>2.0.CO;2.

Marshall, A. G., H. H. Hendon, M. Feng, and A. Schiller, 2015: Initiation and amplification of the Ningaloo Niño. *Climate Dyn.*, **45**, 2367–2385, doi:10.1007/s00382-015-2477-5.

Masumoto, Y., and G. Meyers, 1998: Forced Rossby waves in the southern tropical Indian Ocean. *J. Geophys. Res.*, **103**, 27 589–27 602, doi:10.1029/98JC02546.

McPhaden, M. J., and D. Zhang, 2002: Slowdown of the meridional overturning circulation in the upper Pacific Ocean. *Nature*, **415**, 603–608, doi:10.1038/415603a.

Meyers, G., 1996: Variation of Indonesian Throughflow and the El Niño–Southern Oscillation. *J. Geophys. Res.*, **101**, 12 255–12 263, doi:10.1029/95JC03729.

National Center for Atmospheric Research, 2014: Climate data guide; ORAS4: ECMWF ocean reanalysis and derived ocean heat content. National Center for Atmospheric Research, accessed May 2015. [Available online at https://climatedataguide.ucar.edu/climate-data/oras4-ecmwf-ocean-reanalysis-and-derived-ocean-heat-content.]

Newman, M., and Coauthors, 2016: The Pacific decadal oscillation revisited. *J. Climate*, **29**, 4399–4427, doi:10.1175/JCLI-D-15-0508.1.

Nidheesh, A. G., M. Lengaigne, J. Vialard, A. S. Unnikrishnan, and H. Dayan, 2013: Decadal and long-term sea level variability in the tropical Indo-Pacific Ocean. *Climate Dyn.*, **41**, 381–402, doi:10.1007/s00382-012-1463-4.

Nieves, V., J. K. Willis, and W. C. Patzert, 2015: Recent hiatus caused by decadal shift in Indo-Pacific heating. *Science*, **349**, 532–535, doi:10.1126/science.aaa4521.

Roxy, M. K., K. Ritika, P. Terray, and S. Masson, 2014: The curious case of Indian Ocean warming. *J. Climate*, **27**, 8501–8509, doi:10.1175/JCLI-D-14-00471.1.

Saji, N. H., B. N. Goswami, P. N. Vinayachandran, and T. Yamagata, 1999: A dipole mode in the tropical Indian Ocean. *Nature*, **401**, 360–363.

Schott, F. A., S.-P. Xie, and J. McCreary, 2009: Indian Ocean circulation and climate variability. *Rev. Geophys.*, **47**, RG1002, doi:10.1029/2007RG000245.

Schwarzkopf, F. U., and C. W. Böning, 2011: Contribution of Pacific wind stress to multi-decadal variations in upper-ocean heat content and sea level in the tropical south Indian Ocean. *Geophys. Res. Lett.*, **38**, L12602, doi:10.1029/2011GL047651.

Shi, G., J. Ribbe, W. Cai, and T. Cowan, 2007: Multidecadal variability in the transmission of ENSO signals to the Indian Ocean. *Geophys. Res. Lett.*, **34**, L09706, doi:10.1029/2007GL029528.

Sprintall, J., and A. Revelard, 2014: The Indonesian Throughflow response to Indo-Pacific climate variability. *J. Geophys. Res. Oceans*, **119**, 1161–1175, doi:10.1002/2013JC009533.

——, A. L. Gordon, A. Koch-Larray, T. Lee, J. Potemra, K. Pujiana, and S. E. Wijffels, 2014: The Indonesian Seas and their role in the coupled ocean–climate system. *Nat. Geosci.*, **7**, 487–492, doi:10.1038/ngeo2188.

Stammer, D., M. Balmaseda, P. Heimbach, A. Köhl, and A. Weaver, 2016: Ocean data assimilation in support of climate applications: Status and perspectives. *Annu. Rev. Mar. Sci.*, **8**, 491–518, doi:10.1146/annurev-marine-122414-034113.

Trenary, L. L., and W. Han, 2008: Causes of decadal subsurface cooling in the tropical Indian Ocean during 1961–2000. *Geophys. Res. Lett.*, **35**, L17602, doi:10.1029/2008GL034687.

——, and ——, 2013: Local and remote forcing of decadal sea level and thermocline depth variability in the south Indian Ocean. *J. Geophys. Res. Oceans*, **118**, 381–398, doi:10.1029/2012JC008317.

Ummenhofer, C. C., M. H. England, G. A. Meyers, P. C. McIntosh, M. J. Pook, J. S. Risbey, A. Sen Gupta, and A. S. Taschetto, 2009a: What causes southeast Australia's worst droughts? *Geophys. Res. Lett.*, **36**, L04706, doi:10.1029/2008GL036801.

——, A. Sen Gupta, M. H. England, and C. J. C. Reason, 2009b: Contributions of Indian Ocean sea surface temperatures to enhanced East African rainfall. *J. Climate*, **22**, 993–1013, doi:10.1175/2008JCLI2493.1.

——, ——, A. S. Taschetto, and M. H. England, 2009c: Modulation of Australian precipitation by meridional gradients in east Indian Ocean sea surface temperature. *J. Climate*, **22**, 5597–5610, doi:10.1175/2009JCLI3021.1.

——, ——, Y. Li, A. S. Taschetto, and M. H. England, 2011: Multidecadal modulation of the El Niño–Indian monsoon relationship by Indian Ocean variability. *Environ. Res. Lett.*, **6**, 034006, doi:10.1088/1748–9326/6/3/034006.

——, F. U. Schwarzkopf, G. A. Meyers, E. Behrens, A. Biastoch, and C. W. Böning, 2013: Pacific Ocean contribution to the asymmetry in eastern Indian Ocean variability. *J. Climate*, **26**, 1152–1171, doi:10.1175/JCLI-D-11-00673.1.

Vargas-Hernandez, J. M., S. Wijffels, G. Meyers, and N. J. Holbrook, 2014: Evaluating SODA for Indo-Pacific Ocean decadal climate variability studies. *J. Geophys. Res. Oceans*, **119**, 7854–7868, doi:10.1002/2014JC010175.

——, ——, ——, A. Belo de Couto, and N. Holbrook, 2015: Decadal characterization of Indo-Pacific Ocean subsurface temperature modes in SODA reanalysis. *J. Climate*, **28**, 6113–6132, doi:10.1175/JCLI-D-14-00700.1.

Vialard, J., 2015: Hiatus heat in the Indian Ocean. *Nat. Geosci.*, **8**, 423–424, doi:10.1038/ngeo2442.

Webster, P. J., A. M. Moore, J. P. Loschnigg, and R. R. Leben, 1999: Coupled ocean–atmosphere dynamics in the Indian Ocean during 1997–98. *Nature*, **401**, 356–360, doi:10.1038/43848.

Wijffels, S., and G. Meyers, 2004: An intersection of oceanic waveguides: Variability in the Indonesian Throughflow region. *J. Phys. Oceanogr.*, **34**, 1232–1253, doi:10.1175/1520-0485(2004)034<1232:AIOOWV>2.0.CO;2.

Williams, B., and A. G. Grottoli, 2010: Recent shoaling of the nutricline and thermocline in the western tropical Pacific. *Geophys. Res. Lett.*, **37**, L22601, doi:10.1029/2010GL044867.

Xie, S.-P., H. Annamalai, F. A. Schott, and J. McCreary, 2002: Structure and mechanisms of south Indian Ocean climate variability. *J. Climate*, **15**, 864–878, doi:10.1175/1520-0442(2002)015<0864:SAMOSI>2.0.CO;2.

Yu, L., and R. A. Weller, 2007: Objectively analyzed air–sea heat fluxes for the global ice-free oceans (1981–2005). *Bull. Amer. Meteor. Soc.*, **88**, 527–539, doi:10.1175/BAMS-88-4-527.

——, X. Jin, and R. A. Weller, 2007: Annual, seasonal, and interannual variability of air–sea heat fluxes in the Indian Ocean. *J. Climate*, **20**, 3190–3209, doi:10.1175/JCLI4163.1.